UFSM

CIÊNCIA e NATURA

ISSN 2179-460X
OPEN ACCESS

Ci. e Nat., Santa Maria, e84264, v. 47, 2025 • https://doi.org/10.5902/2179460X84264
Submitted: 27/06/2023 • Approved: 01/08/2024 • Published: 29/04/2025

Chemistry

Synthesis and antimicrobial activity of iron oxide/silver nanocomposites against *Pseudomonas aeruginosa* biofilms

Síntese e atividade antimicrobiana de nanocompósitos de óxido de ferro/prata contra biofilmes de *Pseudomonas aeruginosa*

Aline Fernandes Barcelos[I], Alliny das Graças Amaral[I], Lílian Carla Carneiro[II], Plínio Lázaro Faleiro Naves[I], Luciana Rebelo Guilherme[I]

[I] Universidade Estadual de Goiás, Goiás, GO, Brasil
[II] Universidade Federal de Goiás, Goiás, GO, Brasil

ABSTRACT

Pseudomonas aeruginosa are known for their pathogenicity, antimicrobial resistance, and ability to grow in biofilms, making them even more problematic in health care. In this context, nanotechnology allows the development of new materials against multiresistant microorganisms. The present study prepared colloidal dispersions of iron oxide (IONPs) and silver (AgNPs) nanoparticles and iron oxide/silver composite (IO/Ag-NC), testing them for toxicity and activity against biofilms of *P. aeruginosa* clinical isolates. Heterodimer nanocomposites showed spherical morphology and zeta potential, indicating relative colloidal stability despite their polydispersity. The nanoparticles did not present toxicity to *Artemia salina* at the tested concentrations and inhibited the biofilm formation of some *P. aeruginosa* clinical isolates. Nanoparticles (NPs) inhibited the biofilm formation of some *P. aeruginosa* clinical isolates: AgNPs inhibited biofilm formation in three isolates, IONPs reduced it in four, and IO/Ag-NCs inhibited it in three *P. aeruginosa* isolates. Further research should focus on strategies that consider increasing silver concentration and using IO/Ag-NCs as nanocarriers for controlling microbial biofilm formation.

Keywords: Colloidal dispersion; Heterodimer; *Artemia salina*

RESUMO

As *Pseudomonas aeruginosa* são reconhecidas pela patogenicidade, resistência aos antimicrobianos e habilidade de crescer em biofilmes o que as tornam ainda mais preocupantes na área da saúde. Neste contexto, a nanotecnologia permite o desenvolvimento de novos materiais contra micro-organismos

multirresistentes. No presente trabalho foram preparadas dispersões coloidais de nanopartículas de óxido de ferro (IONPs), prata (AgNPs) e de compósito de óxido de ferro/prata (IO/Ag-NCs) que foram testados quanto à toxicidade e à atividade contra biofilmes de isolados clínicos de *P. aeruginosa*. Os nanocompósitos heterodímeros apresentaram morfologia esférica, potencial zeta indicando relativa estabilidade coloidal apesar da sua polidispersão. As nanopartículas não apresentaram toxicidade para *Artemia salina* nas concentrações testadas e inibiram a formação de biofilmes de alguns dos isolados clínicos de *P. aeruginosa*. As NPs resultaram na inibição da formação de biofilme de alguns dos isolados clínicos de *P. aeruginosa*. As AgNPs inibiram a formação de biofilme em 3 isolados, enquanto as IONPs a reduziram em 4 e as IO/Ag-NCs inibiram em 3 isolados de *P. aeruginosa*. Nossos resultados indicam que novas pesquisas devem ser direcionadas com estratégias que considerem o aumento da concentração de prata e a utilização de IO/Ag-NCs como nanocarreadores para o controle da formação de biofilmes microbianos.

Palavras-chave: Composto híbrido; Heterodímero; *Artemia salina*

1 INTRODUCTION

Individual nanoparticles (NPs) have specific characteristics and applications, such as iron oxide nanoparticles (IONPs) and silver nanoparticles (AgNPs), which individually have antimicrobial properties (Chen et al., 2013; Ismail et al., 2015). The synthesis of nanocomposites containing IONPs and AgNPs (IO/Ag-NCs) combines the characteristics of each nanostructure to improve the applications and limitations of an individual component, including their use in microbial contaminant treatments (Sharma & Jeevanandam, 2013).

In the case of IONPs, they have been tested against the formation of biofilms by microorganisms such as *Staphylococcus aureus*, *Escherichia coli*, *Enterococcus faecalis*, and *Pseudomonas aeruginosa*, and the results of inhibiting the growth of these biofilms have been promising. (Bruckmann et al., 2022). On the other hand, AgNPs can significantly reduce the mass of pathogenic bacteria that are resistant to antibiotics, such as *Burkholderia pseudomallei*, *S. aureus* (ATCC 43300, ATCC 25923 e 29213) e *P. aeruginosa* (ATCC 15442 e ATCC 27853), *E. coli* (ATCC 35218) and *Salmonella Typhi* (ATCC 14028) (Diniz et al., 2020; Hadi et al., 2024; Maheshwari, 2024; Tun et al., 2024).

Bacterial resistance to antimicrobials is a natural phenomenon that may occur due to inappropriately using antibiotics without prescriptions and discontinuing drug

use before the predetermined period (Loureiro et al., 2016). In this context, developing antimicrobial biological agents has become necessary due to the decline of clinically effective antibiotics, especially for refractory biofilm-related infections. Biofilm provides a practical defense against antimicrobial agents, facilitating bacterial spread throughout the patient's body and the development of antimicrobial resistance, such as those from *P. aeruginosa infections* (Ribeiro et al., 2018; Zhang et al., 2020).

P. aeruginosa is a Gram-negative bacterium responsible for hospital infections due to its high adaptability, exhibiting multidrug resistance phenotypes that limit the efficacy of most available antimicrobials. In this context, new methods are required to reduce the morbidity and mortality of patients infected by these microorganisms (Armijo et al., 2020; Boucher et al., 2013; Zamperini et al., 2017).

The lethality test with *Artemia salina* shows a good relationship with other laboratory assays. *A. salina* is a small halophilic invertebrate from the *Crustacea* class and *Brachiopoda* subclass living in saltwater. Its life cycle comprises cyst, nauplii, and metanauplii stages. *A. salina* is highly valued for detecting toxicity through hatched nauplii (lethality assay). The lethality test with *A. salina* is fast, convenient, and inexpensive, thus extensively used in research and applied toxicology (Ntungwe N et al., 2020).

Besides their antimicrobial activity, the toxicity of novel nanoparticles must be assessed, as composite material toxicity may vary from individual components. So, the present study synthesized AgNP, IONP, and IO/Ag-NC colloids and verified nanocomposite toxicity with the *A. salina* lethality assay and antimicrobial activity against biofilms of *P. aeruginosa* clinical isolates.

2 EXPERIMENTS

2.1 Materials

The nanocomposites of IONPs, AgNPs, and IO/Ag-NCs were synthesized using the chemical reagents, $FeCl_2.4H_2O$ (JT Baker, USA), $FeCl_3.6H_2O$ (Neon, Brazil), NH_4OH

(Neon, Brazil), citric acid (Dinâmica, Brazil), $AgNO_3$ (Sigma-Aldrich, USA), sodium citrate (Sigma-Aldrich, India), and $NaBH_4$ (Sigma-Aldrich, USA).

2.2 Synthesis

IONPs were synthesized with the coprecipitation method, according to the methodology by Khalafalla and Reimers (1980). In a beaker, 6 g of $FeCl_2.4H_2O$ and 12 g of $FeCl_3.6H_2O$ were dissolved in 50 mL of deionized water; then, 25 mL of 30% NH_4OH was added by mechanical stirring at 600 rpm. The beaker with the resulting precipitate was separated by magnetic decantation using a permanent neodymium magnet, which helped wash the solid ten times with deionized water (Khalafalla & Reimers, 1980).

IONPs were functionalized by heating a beaker containing the nanoparticles at 60°C with mechanical stirring at 250 rpm. Then, a 0.87 mol L^{-1} citric acid solution was added in drops until reaching a pH of 2.5 to 3.5. The dispersion was washed ten times with deionized water aided by a permanent neodymium magnet. Next, 150 mL of water was added, and NH_4OH was included in drops to reach a pH of 7. A colloid obtained by nanoparticle functionalization was filtered on a 250-nm membrane filter and sterilized in an autoclave.

AgNPs were synthesized by adding 3 mL of a 0.016 mol L^{-1} $AgNO_3$ solution and water up to 200 mL. Then 5 mL of a 0.0054 mol L^{-1} sodium citrate solution was added, starting magnetic stirring and stopping the timer. At 15 minutes, 8 mL were added at a time to the $NaBH_4$ 40 mmol L^{-1} solution stored under refrigeration. At 20 minutes, magnetic stirring stopped, and the reaction mixture remained uncapped in the dark for two hours (Kereselidze et al., 2012). Finally, the resulting colloid was sterilized in an autoclave.

IO/Ag-NC synthesis occurred in a beaker, which received 400 µL of IONPs and 20 mL of deionized water, and 100 mL of an $AgNO_3$ 0.01 mol L^{-1} solution was dripped in the tip sonicator. Subsequently, 400 µL of 1% (w/v) sodium borohydride was added, and the mixture was ultrasonicated for 20 minutes at 40% power. The solution was

heated under vigorous mechanical stirring at 80°C for two hours. The IO/Ag-NCs were washed thrice with deionized water using magnetic decantation (adapted from LIU et al., 2008). Finally, the IO/Ag-NCs were dispersed in water, sterilized in an autoclave, and stored.

2.3 Characterization

Atomic absorption spectroscopy (AAS) identified metal concentrations. For AAS analysis, 100 µL of each nanocomposite sample (IONPs, AgNPs, and IO/Ag-NCs) was opened with concentrated nitric acid. Then, 20 mL of deionized water was added, and the solutions were heated for 20 minutes. Subsequently, the samples were transferred to 100-mL volumetric flasks. The Perkin Elmer AAnalyst 400 atomic absorption spectrophotometer reads the atomic absorptions. IONP samples had 3,560 mg L^{-1} of iron ions, and AgNPs had 100 mg L^{-1} of silver ions. The IO/Ag-NC sample showed iron and silver ion concentrations of 72 and 280 mg L^{-1}, respectively.

Absorption spectroscopy was analyzed in the ultraviolet and visible (UV-vis) region in a Perkin Elmer Lambda 35 UV-Visible Spectrometer equipment. The technique determined optical properties and calculated the samples' band gap (*Eg*) using the Tauc plot in *OriginLab*. *Eg* was determined by extrapolation from the absorption edge provided by the following relationship: $\alpha h\nu = \alpha 0\ (h\nu - Eg)n$. In this equation, $h\nu$ is the energy of incident photons, *Eg* is the optical gap value corresponding to the transitions indicated by n, and $\alpha 0$ is constant depending on the transition probability (Basak et al., 2021). The best linear fit was for n = 2.

Vibrational absorption spectroscopy in the infrared region was analyzed in a Perkin-Elmer Spectrum Frontier FT-IR/NIR (Perkin-Elmer Corp., Norwalk, CT). The samples were prepared on KBr tablets.

The zeta potential and dynamic light scattering (DLS) were examined in a Malvern polystyrene U-shaped cell of the zeta potential in the Malvern ZetaSizer apparatus,

Nano-ZS90 model. The dispersion index (DI) from the DLS analysis was evaluated according to (ISO, 2017).

The samples were analyzed with Transmission Electron Microscopy (TEM) and Selected Area Electron Diffraction (SAED) using the Jeol apparatus, JEM-2100 model, equipped with an energy-dispersive X-ray detector (EDS). The samples' mean diameters and DIs were determined by analyzing the micrographs using ImageJ software.

2.4 *Artemia salina* toxicity test

The method by Molina-Salinas and Said-Fernández (2006), with minor modifications, determined the toxicity of compounds using the *A. salina* lethality assay. The artificial seawater medium (ASM) was prepared by dissolving sea salt (36 g L^{-1}) and yeast extract (6 g L^{-1}) in distilled water, and the solution was sterilized by autoclaving, measuring a pH of 8.5 (Molina-Salinas & Said-Fernández, 2006).

Then, 0.3 g of *A. salina* cysts were incubated in 500 mL of ASM at 25°C for 36 hours under a light shelter with constant oxygenation. After hatching, ten nauplii were attracted with light and transferred in 100 µL of fresh ASM to wells of a microplate previously prepared with 100 µL of nanoparticle dispersions, composing the concentrations of 20.5, 10.25, 5.125, 2.562, and 1.281 µg mL^{-1}. The microplates were incubated at 25°C for 24 hours, and the number of dead and live nauplii per well was counted after this period.

2.5 Biofilm formation inhibition assay of *P. aeruginosa*

Thirteen (13) *P. aeruginosa* were tested: 11 clinical isolates and two American Type Culture Collection (ATCC) strains of *P. aeruginosa* (ATCC 27853 and ATCC 9027) from the laboratory collection.

The bacterial inocula were prepared from colonies grown for 24 hours on cetrimide agar in a sterile physiological solution (0.9% NaCl) with turbidity corresponding

to 0.5 on the McFarland scale. Then, 100 µL of bacterial suspensions were added to 9.9 mL of TSB (trypticase soy broth), and 50 µL aliquots of the broth were transferred to 96-well polystyrene microplate compartments containing the nanocompound samples, an initial inocula of approximately $7.5x10^4$ bacteria, and final concentrations of 0.258 µg mL^{-1} (IONPs), 1 µg mL^{-1} (AgNPs), and 0.258/1 µg mL^{-1} (IO/Ag-NCs) per well.

The microplates were incubated at 35.5ºC for 24 hours and then subjected to visual inspection, growth broth removal, and well washing twice with 150 µL of sterile physiological solution (SPS) in an Aquari® (MA 615, Brazil) automatic microplate washer to remove non-adhered cells. Next, the wells received 150 µL of 1% crystal violet and were washed thrice with 200 µL of distilled water after incubating the dye for 10 minutes, and microplates were dried in an incubator at 35.5ºC for 20 minutes. Finally, each well received 150 µL of absolute ethanol to stain the adhered bacteria, and the microplates were incubated at room temperature for ten minutes to read the optical densities of the wells at 492 nm in the BioTech Epoch™ microplate reader (Naves et al., 2008).

The bacteria were classified for biofilm formation into four categories according to the OD_{CW} (optical density of the control well) and OD_{AB} (optical density of adhered bacteria) ratio, with the following criteria: If $OD_{AB} \leq OD_{CW}$, bacteria are considered non-biofilm formers; if $OD_{AB} > OD_{CW} \leq 2x\ OD_{CW}$, bacteria are weak biofilm formers; if $OD_{AB} > 2x\ OD_{CW} \leq 4X\ OD_{CW}$, bacteria are moderate biofilm formers; and if $OD_{AB} > 4x\ OD_{CW}$, bacteria are strong biofilm formers (Stepanović et al., 2000).

The impact of IONPs, AgNPs, and IO/Ag-NCs on *P. aeruginosa* biofilm formation was evaluated by comparing the results of biofilm formation tests without the nanocomposites (untreated control).

2.6 Statistical analyses

All tests occurred in independent triplicates, and the results were organized by calculating mean and standard deviation values. Nanocomposite toxicity was defined

by calculating the median lethal concentration (LC_{50}) with the number of dead and alive nauplii per well in the *A. salina* lethality assay by Probit analysis with R software. The readings were compared with the untreated viability control to analyze biofilm formation results in the presence of IONPs, AgNPs, and IO/Ag-NCs.

3 RESULTS AND DISCUSSION

3.1 Synthesis and characterization

Figure 1a presents the electronic absorption spectra in the ultraviolet and visible (UV-vis) region of the prepared colloidal dispersions (IONPs, AgNPs, and IO/Ag-NCs). The IONP spectrum shows a broadband bandwidth between 200 and 350 nm, indicating a very energetic band and charge transfer transition (Litter & Blesa, 1992). The image also presents an intense plasmonic band centered at 395 nm for AgNPs, confirming AgNP formation and suggesting a spherical and regular shape (Shervani et al., 2008).

The IO/Ag-NC spectrum suggests that the synthesized nanocomposite comprises silver and iron oxide nanoparticles. This spectrum shows two bands: one centered at 277 nm and another quite intense band centered at 431 nm. The former can be attributed to IONPs and suggests charge transfer transition (Kumar et al., 2014; Litter & Blesa, 1992), and the latter corresponds to a plasmonic band typical of silver nanoparticles with irregular shapes (Shervani et al., 2008)

Figures 1b, 1c, and 1d present Tauc plot extrapolations to determine the optical gap value of the samples. IONP (Figure 1b) and AgNP (Figure 1c) samples obtained optical gaps of 3.37 eV and 2.75 eV, respectively. These results were consistent with the literature, which identified values of 2.51 eV for AgNPs (Aziz et al., 2018) and 3.5 eV and 3.23 eV for IONPs (Basak et al., 2021). Figure 1d shows two optical gaps for IO/Ag-NCs (2.3 and 3.9 eV), with displaced values of individual AgNPs and IONPs, respectively. These values suggest that the gap energy in

the nanocomposite decreases for AgNPs, shifting the plasmonic band to longer wavelengths (Caro et al., 2016; Sallam et al., 2018). The results indicate that the samples are semiconducting compounds and may serve as catalysts.

Figure 1 – a) Electronic absorption spectra in the UV-vis region; b) Tauc Plot of IONPs; c) Tauc Plot of AgNPs; and d) Tauc Plot of IO/Ag-NCs

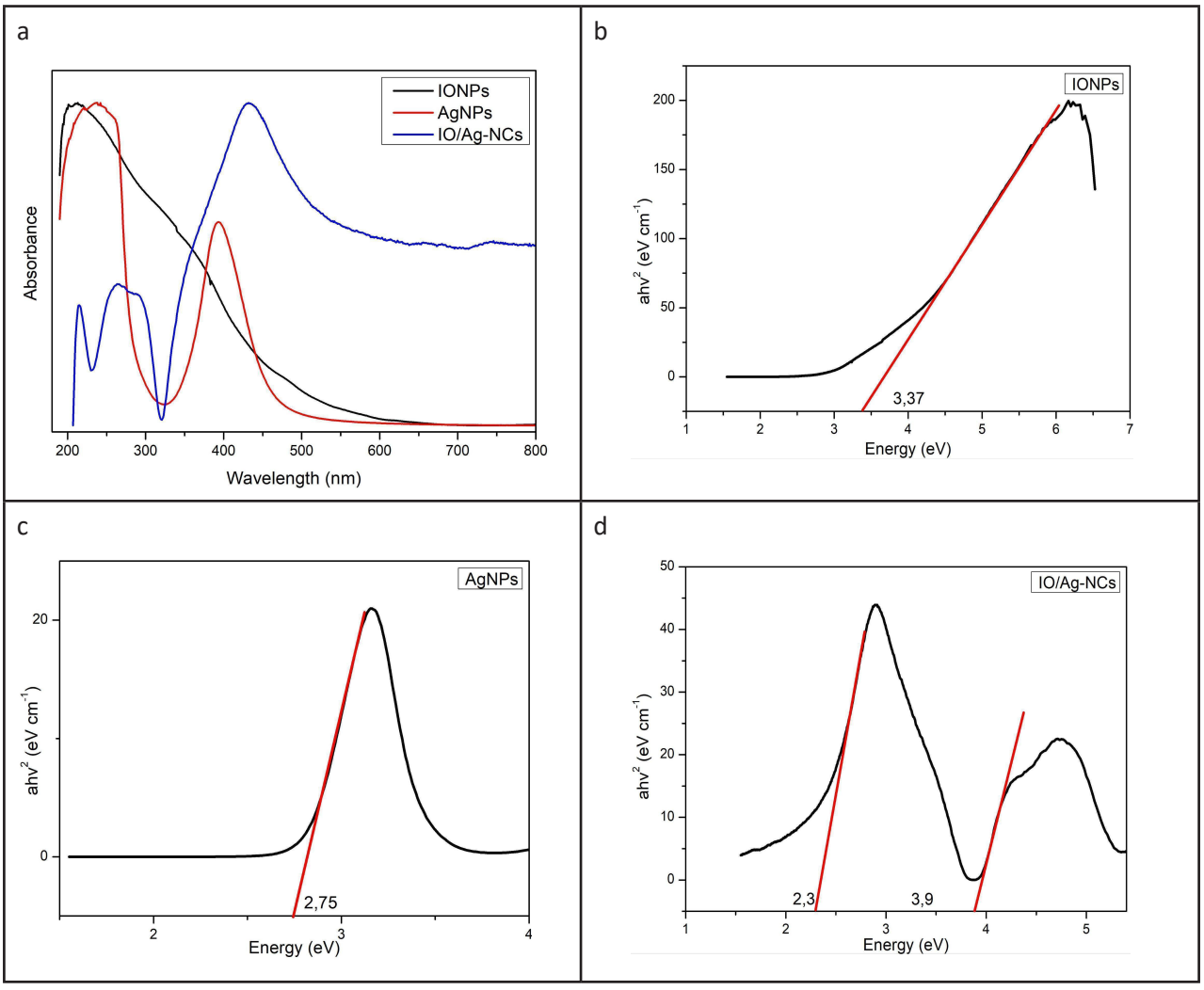

Source: authors (2023)

Figure 2 shows the FTIR analysis spectra for NP samples in the 4,000 to 400 cm^{-1} region. IONP, AgNP, and IO/Ag-NC samples have bands in the region of 3,450 cm^{-1}. Bands in the region of 3,400 cm^{-1} refer to O-H bond stretching due to moisture. The samples show bands in the region of 1,630 cm^{-1}, and the absorption in the range of 1,715 ± 100 cm^{-1} is usually due to the C-O bond (carbonyl group) in molecules. All

samples also presented bands in the region of 1,400 cm^{-1}, and the absorption in this region refers to the CH_2 folding in citric acid and sodium citrate used to synthesize NPs (Pavia et al., 2010).

Figure 2 - FTIR spectra of nanocomposites

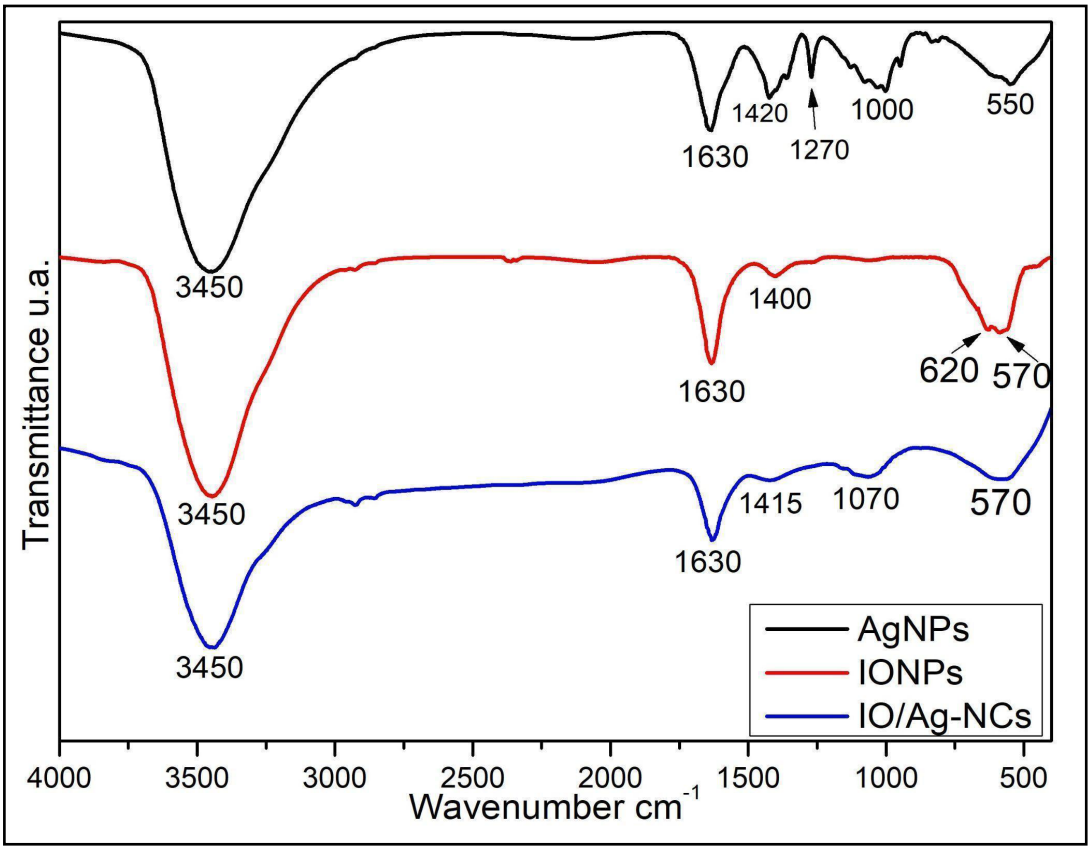

Source: authors (2023)

The band (Figure 2) at approximately 1,270 cm^{-1} corresponds to the C-O bond stretching in citric acid and sodium citrate used to synthesize NPs. The bands between 1,000 and 400 cm^{-1} of the AgNP spectrum are characteristic of C-H bond deformation and out-of-plane bending of C-H and CH2 (Pavia et al., 2010).

The high-intensity bands in the region of 600 cm^{-1} in the IONP and IO/Ag-NC spectrum are typical of Fe-O stretching in inverse spinel iron oxide. Two bands around 630 and 590 cm^{-1} represent the y-Fe_2O_3 (maghemite) Fe-O bond (Karimzadeh et al., 2016; Wang et al., 2014). Thus, the bands in the 620 and 570 cm^{-1} FTIR spectrum suggest that the IONPs in this study are maghemite.

Table 1 shows the results of IONP, AgNP, and IO/Ag-NC characterizations by zeta potential, hydrodynamic radius, and dispersion index (DI). IONPs and AgNPs presented hydrodynamic radii of 106.7 nm and 63.27 nm and DIs of 0.159 and 0.491, respectively. Thus, the DI data of the samples indicated IONPs with homogeneous size dispersions and AgNPs with inhomogeneous size dispersions. IONPs and AgNPs also presented zeta potentials of -37.7 mV and -43.5 mV, respectively, which are highly stable (as a rule of thumb, the potentials above +30 or below -30 mV are considered highly stable) (Makowski et al., 2019).

According to the ISO 22412 (2017), the DI of the samples indicated inhomogeneous size dispersions for IO/Ag-NCs, which showed hydrodynamic radii of 443.2 and 573.9 nm and DIs of 0.645 (based on the refractive index of iron oxide) and 0.806 (based on the refractive index of silver) for iron oxide and silver analyses. IO/Ag-NCs also showed zeta potentials of -21.9 mV and -15.1 mV for iron oxide and silver analyses, respectively. The zeta potential values of IO/Ag-NCs indicate instability, as they are outside, above, or below ± 30 mV, which suggests high colloidal system stability (Makowski et al., 2019).

Table 1 – Nanocomposite characterizations by zeta potential and DLS

Nanocompounds	Zeta potential (mV)	Hydrodynamic size (nm)	Polydispersity index - PI	Refractive index (n)
IONPs	-37.7 ± 12.1	106.7	0.159	2.33
AgNPs	-43.5 ± 14.6	63.27	0.491	0.54
IO/Ag-NCs	-21.9 ± 5.70 / -15.1 ± 5.68	443.2 / 573.9	0.645 / 0.806	2.33 / 0.54

Source: authors (2023)

Figure 3 presents the transmission electron microscopy (TEM) micrographs, nanoparticle diameter distribution plots, and selected area electron diffraction (SAED) of the samples of (a) IONPs, (b) AgNPs, and (c) IO/Ag-NCs. The IONP micrographs show spherical NPs, the AgNP micrographs present spherical and oval NPs, and the IO/Ag-NC micrographs demonstrate spherical (O), oval (0), and hexagonal (⬡) NPs.

Figure 3 – Micrographs, diameter distribution histogram, and SAED of a) IONPs, b) AgNPs, and c) IO/Ag-NCs. Spherical (O), oval (0), and hexagonal (⬡) surround particles with corresponding shapes

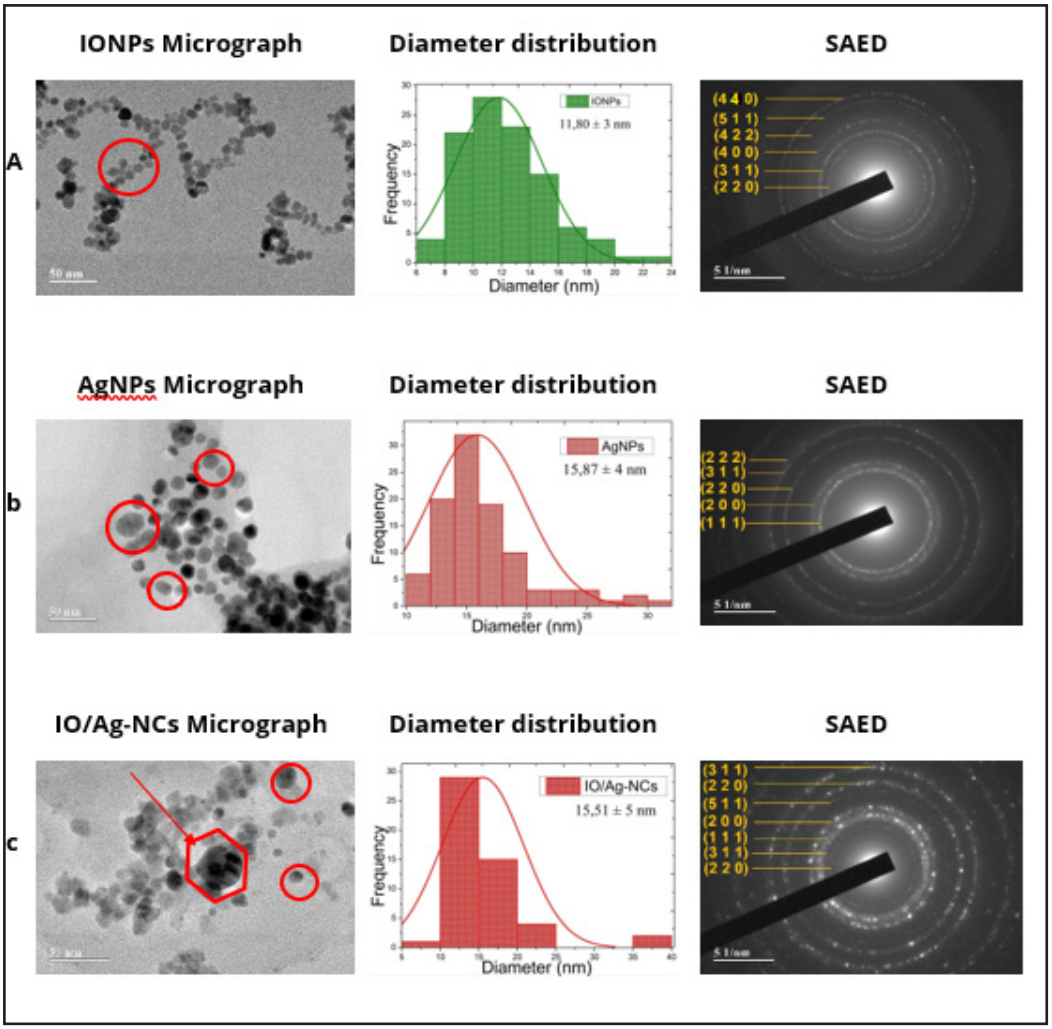

Source: authors (2023)

Figure 3(a) of the IONPs micrograph indicates that NPs may bond potentially through NP functionalization with citric acid, as the functionalized citrate ions bonded by cross-linking on IONP surfaces.

Figure 3(b) indicates the aggregation state for AgNPs, as the image shows NPs partially dispersed and partially aggregated, confirming the DLS and zeta potential analysis data that show little homogeneity for AgNPs.

Figure 3(c) presents IO/Ag-NC NPs with a layer in different directions, suggesting NC formations. However, the growth of NCs may have increased the aggregation state of the particles, as confirmed by DLS and zeta potential analyses. IO/Ag-NC micrographs suggest a heterodimer characteristic, as IONPs are directly attached to the silver surface but do not cover it completely.

The ImageJ program found mean diameters of 11.80 ± 3 nm, 15.87 ± 4 nm, and 15.51 ± 5 nm for IONPs, AgNPs, and IO/Ag-NCs, respectively. The size distribution histograms in Figure 3 represents these values. This analysis provides size distributions of NPs from TEM images, with information about mean sizes and standard deviations. The mean diameter found was expected according to the data for iron oxide in the literature (Bhattacharjee, 2016; Kim et al., 2015; Zhao et al., 2015).

Sonbol, Mohammed, and Korany (2022) synthesized AgNPs using the *Phoma* sp, *Chaetomium globosum,* and *Chaetomium* sp fungal isolates as silver-reducing agents. They calculated the particle size distribution of TEM images using the ImageJ program. Furthermore, their study showed mean sizes of 12.7, 10.7, and 16.1 nm for the three mentioned syntheses. As for the DLS analysis, the hydrodynamic radii of the particles were 98.41, 83.15, and 51.76 nm (Sonbol et al., 2022).

The SAED analysis evaluates the crystalline structure of biomaterials through the pattern of diffraction points obtained in TEM analyses. The d-spacing patterns of AgNPs and IONPs were considered to find the same patterns in NCs. Table 2 shows the peaks of the known d-spacing values representing the crystallographic plane.

Planes [220], [311], [400], [422], [511], and [440]/[214] (Figure 3(a)) and [111], [200], [220], [311], and [222] (Figure 3(b)) were found for IONPs and AgNPs, respectively. Consequently, d-spacing values showed the following planes representing silver and iron oxide in IO/Ag-NCs: [220], [311], [111], [200], [511], [220], and [311] (Figure 3(c)) (Galateanu et al., 2015; Mehtab et al., 2018; Njagi et al., 2011).

Table 2 – Miller indices of known d-spacing values for AgNPs, IONPs, and IO/Ag-NCs

Planes	AgNPs *d-spacing*	IONPs *d-spacing*	IO/Ag-NCs *d-spacing*
[220]		2.968239834	2.842524161
[311]		2.531966072	2.444390125
[111]	2.251491613		2.232392008
[400]		2.105484788	
[200]	1.948368242		1.985111663
[422]		1.733102253	
[511]		1.630656339	1.583155228
[440] [214]		1.487099413	
[220]	1.380357513		1.401345291
[311]	1.191043354		1.189909567
[222]	1.117505727		

Source: authors (2023)

The AgNP planes were considered typical values of face-centered cubic structures. Silver showed no extra diffraction peaks, suggesting it is pure. These NPs with high purity and low toxicity are attractive for biological applications (Mehtab et al., 2018; Njagi et al., 2011).

The IONPs showed a d-spacing pattern of 1.48. Noval and Carriazo (2019) consider this pattern a reference to the 440 (Fe_3O_4) and 214 (α-Fe_2O_3) planes, suggesting the presence of hematite in IONP dispersions. IO/Ag-NCs showed diffraction peaks of both NPs, indicating their presence in the sample (Noval & Carriazo, 2019).

AgNPs are highly crystalline, with diffraction peaks corresponding to the face-centered cubic phase, agreeing with the reported ICDD 4-783; a = 4.0862Å. The analysis indicates a nanocrystalline sample with IONP indexing as a cubic crystalline network with surfaces according to ICDD file number 04-008-8146 (Galateanu et al., 2015; Njagi et al., 2011).

3.2 *Artemia salina* toxicity test

AgNPs, IONPs, and IO/Ag-NCs showed no toxicity to *A. salina*, as there was no LC_{50} at the tested concentrations. The lethal dose of NPs is higher than the highest

evaluated concentration (20.5 μg mL^{-1}). The limiting factor was that AgNPs have a maximum concentration of 100 μg mL^{-1}, making it hard to test higher concentrations than the maximum one used in microdilution tests.

A previous study on AgNP toxicity in *A. salina* nauplii, under ISO TS 20787 guidelines, exposed nauplii to 0 (untreated control), 0.39, 1.56, 6.25, 25, and 100 mg L^{-1} for 24, 48, and 72 hours. The results indicated a low immobilization rate of nauplii within 24 hours, and their immobilization in a concentration-dependent manner occurred only after 72 hours. Thus, in 24 hours, the maximum tested concentration was insufficient to immobilize the nauplii (An et al., 2019).

The *A. salina* lethality test correlates well with more complex tests in determining antifungal, antiviral, and antimicrobial activities, among others. It is also an inexpensive and easily interpreted test extensively used to screen bioactive compounds (Krishnaraju et al., 2005; Luna et al., 2005; Pisutthanan et al., 2004).

3.3 Nanocomposite activity on biofilm formation of *P. aeruginosa*

All 13 *P. aeruginosa* formed biofilms, of which nine (69.23%) were classified as strong biofilm formers and four (30.77%) as moderate biofilm formers. The impact of nanocomposites on *P. aeruginosa* biofilm formation occurred variably and depended on clinical isolates.

IONPs reduced biofilm formation for Pa3, Pa11, Pa22, and Pa23 isolates; AgNPs decreased it for Pa3, and Pa11; and IO/Ag-NCs reduced it for Pa3, Pa11, Pa22, Pa23, and Pa28. However, IONPs increased biofilm formation for Pa5, Pa13, Pa ATCC 9027, and Pa ATCC 27853; AgNPs increased for Pa13, Pa20, Pa28, Pa29, and Pa ATCC 9027; while IO/Ag-NCs increased for Pa10, Pa13, Pa20, Pa29, Pa ATCC 9027, and Pa ATCC 27853. For the other bacteria, under the same treatment conditions, biofilm formation did not significantly decrease or increase (Figure 4).

Figure 4 – Biofilm formation of *P. aeruginosa* clinical isolates in the presence of a) IONPs (0.258 μg mL^{-1}), b) AgNPs (1 μg mL^{-1}), and c) IO/Ag-NCs (0.258/1 μg mL^{-1}) compared to untreated controls (UC)

Source: authors (2023)

The size of AgNPs is crucial in antibiofilm activity against multidrug-resistant *P. aeruginosa* because smaller particles have a more significant surface area contact with the microorganism. Antibiofilm activity occurs through Bi structure disruption and oxidative stress. Using AgNPs is promising for developing new antimicrobial systems against *P.* aeruginosa strains (de Lacerda Coriolano et al., 2021).

IONP diameters significantly influence the inhibition of bacterial biofilm formation (Sathyanarayanan et al., 2013). Our study found that IONPs with a diameter of 11.80 ± 3 nm at a concentration of 0.258 μg mL^{-1} inhibited biofilm formation in four of the analyzed isolates (Pa3, Pa11, Pa22, and Pa23).

A previous study showed that IONPs with diameters smaller than 10 nm, besides the dispersion concentration, significantly inhibited the growth of bacterial biofilms. IONPs at 10 μg mL^{-1} can impact *P. aeruginosa* biofilm growth, but only concentrations higher than 50 μg mL^{-1} significantly inhibited biofilm formation (Sathyanarayanan et al., 2013).

Zinc oxide NPs (~20 nm) at 350 μg mL^{-1} reduced biofilm formation by more than 94% in 15 *P. aeruginosa* clinical isolates ATCC 9027 (da Silva Bruckmann et al., 2022). In another study, AgNPs showed minimum inhibitory concentrations (MICs) of 1.406 - 5.625 μg mL^{-1} against multidrug-resistant *P. aeruginosa* in a concentration-dependent manner (Liao et al., 2019).

NCs can improve the stability and antimicrobial activity of AgNPs (known and extensively studied in antimicrobial testing) (Prabhu & Poulose, 2012; Zhang et al., 2020). Contrarily, our results indicate that IO/Ag-NCs did not increase the inhibition of *P. aeruginosa* biofilm formation. However, isolated AgNPs inhibited identical isolates, except for Pa28, which was affected only by IO/Ag-NCs.

Chitosan (CS) and zinc oxide (ZnO) nanocomposites with and without gentamicin were tested at concentrations lower than the MIC against *P. aeruginosa* PAO1 biofilms and provided significant reductions ($p < 0.05$). The MIC of 128 μg mL^{-1} of CS-ZnO NCs

showed a 63% biofilm reduction, and CS-ZnO NCs with gentamicin at 0.5 μg mL^{-1} dramatically reduced biofilm formation by 84% (Hemmati et al., 2020).

The tested nanocomposites did not reduce biofilm formation for all isolates: AgNPs did not inhibit biofilm formation for Pa28 and Pa ATCC 9027 isolates (Figure 4a), IO/Ag-NCs did not reduce it for Pa20, Pa ATCC 9027, and Pa ATCC 27853 (Figure 4b), and IONPs did not inhibit it for Pa5 and Pa ATCC 9027 (Figure 4c).

However, concentrations higher than the one tested in our study (1 μg mL^{-1}) significantly reduced *P. aeruginosa* biofilm formation (da Silva Bruckmann et al., 2022; Hemmati et al., 2020; Sathyanarayanan et al., 2013).

4 CONCLUSIONS

The prepared IO/Ag-NCs were particles with spherical morphology commonly presenting aggregates, suggesting that functionalization caused the aggregate state. However, the formed colloid was stable under the tested conditions, showing a high zeta potential value. The synthesized IONPs and AgNPs were particles with spherical morphology, a few aggregates, and a high zeta potential value, suggesting particle stability.

NPs showed no toxicity at the maximum LC_{50} of 20.5 μg mL^{-1} for *A. salina*. They inhibited biofilm formation in some *P. aeruginosa* clinical isolates. AgNPs inhibited biofilm formation in three isolates, IONPs reduced it in four, and IO/Ag-NCs inhibited it in three *P. aeruginosa* isolates.

The non-toxicity of NPs and biofilm formation results indicate that further research should be performed with higher silver concentrations and using IO/Ag-NCs as nanocarriers for a controlled and targeted drug release by combining the magnetic property of IONPs with the antimicrobial property of AgNPs.

ACKNOWLEDGMENTS

The authors would like to thank the Universidade Estadual de Goiás (UEG) for the master scholarship's financial support. Also, to the Centro de Análises, Inovação e Tecnologia Universidade Estadual de Goiás (CAITec-UEG), the Multi-user Analysis Center (CAM-UFG), and Multi-user Laboratory of High-Resolution Microscopy (Labmic – UFG) for the TEM images. For the financial support to Universidade Estadual de Goiás Edital PRÓ-PROJETOS PESQUISA n.005/2021.

REFERENCES

An, H. J., Sarkheil, M., Park, H. S., Yu, I. J., & Johari, S. A. (2019). Comparative toxicity of silver nanoparticles (AgNPs) and silver nanowires (AgNWs) on saltwater microcrustacean, Artemia salina. *Comparative Biochemistry and Physiology Part - C: Toxicology and Pharmacology*, *218*. https://doi.org/10.1016/j.cbpc.2019.01.002

Armijo, L. M., Wawrzyniec, S. J., Kopciuch, M., Brandt, Y. I., Rivera, A. C., Withers, N. J., Cook, N. C., Huber, D. L., Monson, T. C., Smyth, H. D. C., & Osiński, M. (2020). Antibacterial activity of iron oxide, iron nitride, and tobramycin conjugated nanoparticles against *Pseudomonas aeruginosa* biofilms. *Journal of Nanobiotechnology*, *18*(1). https://doi.org/10.1186/s12951-020-0588-6

Aziz, Khalid, M., Akhtar, M. S., Nadeem, M., Gilani, Z. A., Ul Huda Khan Asghar, H. M. N., Rehman, J., Ullah, Z., & Saleem, M. (2018). Structural, morphological and optical investigations of silver nanoparticles synthesized by sol-gel auto-combustion method. *Journal of Nanomaterials and Biostructures*, *13*(3).

Basak, S., Ali, S., Das, D., Mondal, M., Dutta, A., Kumar, A., Sikdar, S., & Roy, M. N. (2021). Green Synthesis of Iron Oxide Nanoparticles to Explore Cytotoxic Behaviour and to Diminish Environmental Pollution by a Novel Contrivance. *Journal of Chemical, Biological and physical sciences*, *11*(1), 147–170. https://doi.org/10.24214/jcbps.A.11.1.14770

Bhattacharjee, S. (2016). DLS and zeta potential–what they are and what they are not? *Journal of controlled release*, *235*, 337–351.

Boucher, H. W., Talbot, G. H., Benjamin Jr, D. K., Bradley, J., Guidos, R. J., Jones, R. N., Murray, B. E., Bonomo, R. A., Gilbert, D., & America, I. D. S. of. (2013). 10×'20 progress—development of new drugs active against gram-negative bacilli: an update from the Infectious Diseases Society of America. *Clinical infectious diseases*, *56*(12), 1685–1694.

Bruckmann, F. da S., Viana, A. R., Lopes, L. Q. S., Santos, R. C. V., Muller, E. I., Mortari, S. R., & Rhoden, C. R. B. (2022). Synthesis, Characterization, and Biological Activity Evaluation of Magnetite-Functionalized Eugenol. *Journal of Inorganic and Organometallic Polymers and Materials*, *32*(4), 1459–1472. https://doi.org/10.1007/s10904-021-02207-7

Caro, C., Sayagues, M. J., Franco, V., Conde, A., Zaderenko, P., & Gámez, F. (2016). A hybrid silver-magnetite detector based on surface enhanced Raman scattering for differentiating organic compounds. *Sensors and Actuators B: Chemical*, *228*, 124–133.

Chen, Y., Gao, N., & Jiang, J. (2013). Surface matters: Enhanced bactericidal property of core-shell Ag-Fe_2O_3 nanostructures to their heteromer counterparts from one-pot synthesis. *Small*, *9*(19). https://doi.org/10.1002/smll.201300543

da Silva Bruckmann, F., Viana, A. R., Lopes, L. Q. S., Santos, R. C. V., Muller, E. I., Mortari, S. R., & Rhoden, C. R. B. (2022). Synthesis, Characterization, and Biological Activity Evaluation of Magnetite-Functionalized Eugenol. *Journal of Inorganic and Organometallic Polymers and Materials*, *32*(4), 1459–1472. https://doi.org/10.1007/s10904-021-02207-7

de Lacerda Coriolano, D., de Souza, J. B., Bueno, E. V., Medeiros, S. M. de F. R., Cavalcanti, I. D. L., & Cavalcanti, I. M. F. (2021). Antibacterial and antibiofilm potential of silver nanoparticles against antibiotic-sensitive and multidrug-resistant *Pseudomonas aeruginosa* strains. *Brazilian Journal of Microbiology*, *52*(1), 267–278. https://doi.org/10.1007/s42770-020-00406-x

Diniz, F. R., Maia, R. C. A. P., de Andrade, L. R. M., Andrade, L. N., Vinicius Chaud, M., da Silva, C. F., Corrêa, C. B., de Albuquerque Junior, R. L. C., Pereira da Costa, L., & Shin, S. R. (2020). Silver nanoparticles-composing alginate/gelatine hydrogel improves wound healing in vivo. *Nanomaterials*, *10*(2), 390.

Galateanu, B., Bunea, M.-C., Stanescu, P., Vasile, E., Casarica, A., Iovu, H., Hermenean, A., Zaharia, C., & Costache, M. (2015). *In vitro* studies of bacterial cellulose and magnetic nanoparticles smart nanocomposites for efficient chronic wounds healing. *Stem cells international*, *2015*.

Hadi, A. A., Nizam, A., Malek, N., Matmin, J., Asraf, M. H., Susanto, H., Din, S. M., & Shamsuddin, M. (2024). Synergistic antibacterial effect of Persicaria odorata synthesised silver nanoparticles with antibiotics on drug-resistant bacteria. *Inorganic Chemistry Communications*, *159*, 111725. https://doi.org/10.1016/j.inoche.2023.111725

Hemmati, F., Salehi, R., Ghotaslou, R., Kafil, H. S., Hasani, A., Gholizadeh, P., & Rezaee, M. A. (2020). The assessment of antibiofilm activity of chitosan-zinc oxide-gentamicin nanocomposite on *Pseudomonas aeruginosa* and *Staphylococcus aureus*. *International Journal of Biological Macromolecules*, *163*, 2248–2258.

Ismail, R. A., Sulaiman, G. M., Abdulrahman, S. A., & Marzoog, T. R. (2015). *Antibacterial activity of magnetic iron oxide nanoparticles synthesized by laser ablation in liquid*. https://doi.org/10.1016/j.msec.2015.04.047

ISO, I. S. O. (2017). 22412: 2017 Particle size analysis—Dynamic light scattering (DLS). *International Organization for Standardization: Geneva, Switzerland*.

Karimzadeh, I., Dizaji, H. R., & Aghazadeh, M. (2016). Preparation, characterization and PEGylation of superparamagnetic Fe_3O_4 nanoparticles from ethanol medium via cathodic electrochemical deposition (CED) method. *Materials Research Express*, *3*(9), 095022.

Kereselidze, Z., Romero, V. H., Peralta, X. G., & Santamaria, F. (2012). Gold nanostar synthesis with a silver seed mediated growth method. *JoVE (Journal of Visualized Experiments)*, *59*, e3570.

Khalafalla, S., & Reimers, G. (1980). Preparation of dilution-stable aqueous magnetic fluids. *IEEE Transactions on Magnetics*, *16*(2), 178–183. https://doi.org/10.1109/TMAG.1980.1060578

Kim, K.-H., Xing, H., Zuo, J.-M., Zhang, P., & Wang, H. (2015). TEM based high resolution and low-dose scanning electron nanodiffraction technique for nanostructure imaging and analysis. *Micron*, *71*, 39–45.

Krishnaraju, A. V, Rao, T. V. N., Sundararaju, D., Vanisree, M., Tsay, H.-S., & Subbaraju, G. V. (2005). Assessment of bioactivity of Indian medicinal plants using brine shrimp (*Artemia salina*) lethality assay. *International Journal of Applied Science and Engineering*, *3*(2), 125–134.

Kumar, B., Smita, K., Cumbal, L., & Debut, A. (2014). Biogenic synthesis of iron oxide nanoparticles for 2-arylbenzimidazole fabrication. *Journal of Saudi Chemical Society*, *18*(4), 364–369.

Liao, S., Zhang, Y., Pan, X., Zhu, F., Jiang, C., Liu, Q., Cheng, Z., Dai, G., Wu, G., & Wang, L. (2019). Antibacterial activity and mechanism of silver nanoparticles against multidrug-resistant *Pseudomonas aeruginosa*. *International journal of nanomedicine*, 1469–1487.

Litter, M. I., & Blesa, M. A. (1992). Photodissolution of iron oxides. IV. A comparative study on the photodissolution of hematite, magnetite, and maghemite in EDTA media. *Canadian Journal of Chemistry*, *70*(9), 2502–2510.

Liu, C. H., Zhou, Z. D., Yu, X., Lv, B. Q., Mao, J. F., & Xiao, D. (2008). Preparation and characterization of Fe_3O_4/Ag composite magnetic nanoparticles. *Inorganic materials*, *44*, 291–295.

Loureiro, R. J., Roque, F., Rodrigues, A. T., Herdeiro, M. T., & Ramalheira, E. (2016). O uso de antibióticos e as resistências bacterianas: breves notas sobre a sua evolução. *Revista Portuguesa de saúde pública*, *34*(1), 77–84.

Luna, J. de S., Dos Santos, A. F., De Lima, M. R. F., De Omena, M. C., De Mendonça, F. A. C., Bieber, L. W., & Sant'Ana, A. E. G. (2005). A study of the larvicidal and molluscicidal activities of some medicinal plants from northeast Brazil. *Journal of Ethnopharmacology*, *97*(2), 199–206.

Maheshwari, S. (2024). Synergistic effects of *Woodfordia fruticosa* silver nanoparticles accelerating wound healing in Swiss mice *in vivo*. *Intelligent Pharmacy*, *2*(1), 17–27.

Makowski, M., Silva, Í. C., Pais do Amaral, C., Gonçalves, S., & Santos, N. C. (2019). Advances in lipid and metal nanoparticles for antimicrobial peptide delivery. *Pharmaceutics*, *11*(11), 588.

Mehtab, S., Zaidi, M. G. H., & Irshad Siddiqi, T. (2018). Designing Fructose Stabilized Silver Nanoparticles for Mercury(II) Detection and Potential Antibacterial Agents. *Material Science Research India*, *15*(3), 241–249. https://doi.org/10.13005/msri/150305

Molina-Salinas, G. M., & Said-Fernández, S. (2006). A modified microplate cytotoxicity assay with brine shrimp larvae (*Artemia salina*). *Pharmacologyonline*, *3*, 633–638.

Naves, P., del Prado, G., Huelves, L., Gracia, M., Ruiz, V., Blanco, J., Dahbi, G., Blanco, M., del Carmen Ponte, M., & Soriano, F. (2008). Correlation between virulence factors and in vitro biofilm formation by *Escherichia coli* strains. *Microbial pathogenesis*, *45*(2), 86–91.

Njagi, E. C., Huang, H., Stafford, L., Genuino, H., Galindo, H. M., Collins, J. B., Hoag, G. E., & Suib, S. L. (2011). Biosynthesis of iron and silver nanoparticles at room temperature using aqueous sorghum bran extracts. *Langmuir*, *27*(1), 264–271.

Noval, V. E., & Carriazo, J. G. (2019). Fe_3O_4-TiO_2 and Fe_3O_4-SiO_2 core-shell powders synthesized from industrially processed magnetite (Fe_3O_4) microparticles. *Materials Research*, *22*, e20180660.

Ntungwe N, E., Domínguez-Martín, E. M., Roberto, A., Tavares, J., Isca, V., Pereira, P., Cebola, M.-J., & Rijo, P. (2020). Artemia species: An important tool to screen general toxicity samples. *Current Pharmaceutical Design*, *26*(24), 2892–2908.

Pavia, D. L., Lampman, G. M., Kriz, G. S., & Vyvyan, J. R. (2010). Introdução à espectroscopia: Tradução da 4ª edição Norte-Americana. Em P. Barros (Org.), *São Paulo: Cengage Learning* (4º ed). Cengage Learning.

Pisutthanan, S., Plianbangchang, P., Pisutthanan, N., Ruanruay, S., & Muanrit, O. (2004). Brine shrimp lethality activity of Thai medicinal plants in the family *Meliaceae*. *Naresuan University Journal: Science and Technology (NUJST)*, *12*(2), 13–18.

Prabhu, S., & Poulose, E. K. (2012). Silver nanoparticles: mechanism of antimicrobial action, synthesis, medical applications, and toxicity effects. *International nano letters*, *2*, 1–10.

Ribeiro, K. L., Frías, I. A. M., Franco, O. L., Dias, S. C., Sousa-Junior, A. A., Silva, O. N., Bakuzis, A. F., Oliveira, M. D. L., & Andrade, C. A. S. (2018). Clavanin A-bioconjugated Fe_3O_4/Silane core-shell nanoparticles for thermal ablation of bacterial biofilms. *Colloids and Surfaces B: Biointerfaces*, *169*, 72–81.

Sallam, S. A., El-Subruiti, G. M., & Eltaweil, A. S. (2018). Facile synthesis of Ag–γ-Fe_2O_3 superior nanocomposite for catalytic reduction of nitroaromatic compounds and catalytic degradation of methyl orange. *Catalysis Letters*, *148*, 3701–3714.

Sathyanarayanan, M. B., Balachandranath, R., Genji Srinivasulu, Y., Kannaiyan, S. K., & Subbiahdoss, G. (2013). The effect of gold and iron-oxide nanoparticles on biofilm-forming pathogens. *International Scholarly Research Notices*, *2013*.

Sharma, G., & Jeevanandam, P. (2013). A facile synthesis of multifunctional iron oxide@ Ag core–shell nanoparticles and their catalytic applications. *European Journal of Inorganic Chemistry*, *2013*(36), 6126–6136.

Shervani, Z., Ikushima, Y., Sato, M., Kawanami, H., Hakuta, Y., Yokoyama, T., Nagase, T., Kuneida, H., & Aramaki, K. (2008). Morphology and size-controlled synthesis of silver nanoparticles in aqueous surfactant polymer solutions. *Colloid and Polymer Science*, *286*, 403–410.

Sonbol, H., Mohammed, A. E., & Korany, S. M. (2022). Soil fungi as biomediator in silver nanoparticles formation and antimicrobial efficacy. *International Journal of Nanomedicine*, 2843–2863.

Stepanović, S., Vuković, D., Dakić, I., Savić, B., & Švabić-Vlahović, M. (2000). A modified microtiter-plate test for quantification of staphylococcal biofilm formation. *Journal of microbiological methods*, *40*(2), 175–179.

Tun, W. S. T., Hongsing, N., Sirithongsuk, P., Nasompak, S., Daduang, S., Klaynongsruang, S., Taweechaisupapong, S., Chareonsudjai, S., Prangkio, P., & Kosolwattana, S. (2024). The synergistic action of silver nanoparticles and ceftazidime against antibiotic-resistant *Burkholderia pseudomallei*: A modifying treatment. *Process Biochemistry*, *136*, 351–361.

Wang, F., Yin, C., Wei, X., Wang, Q., Cui, L., Wang, Y., Li, T., & Li, J. (2014). Synthesis and characterization of superparamagnetic Fe_3O_4nanoparticles modified with oleic acid. *Integrated Ferroelectrics*, *153*(1), 92–101.

Zamperini, C., Maccari, G., Deodato, D., Pasero, C., D'Agostino, I., Orofino, F., De Luca, F., Dreassi, E., Docquier, J.-D., & Botta, M. (2017). Identification, synthesis and biological activity of alkyl-guanidine oligomers as potent antibacterial agents. *Scientific reports*, *7*(1), 8251.

Zhang, Y., Pan, X., Liao, S., Jiang, C., Wang, L., Tang, Y., Wu, G., Dai, G., & Chen, L. (2020). Quantitative proteomics reveals the mechanism of silver nanoparticles against multidrug-resistant *Pseudomonas aeruginosa* biofilms. *Journal of proteome research*, *19*(8), 3109–3122.

Zhao, X., Zhu, S., Song, Y., Zhang, J., & Yang, B. (2015). Thermal responsive fluorescent nanocomposites based on carbon dots. *RSC advances*, *5*(20), 15187–15193.

Authorship contributions

1 – Aline Fernandes Barcelos

Master in Sciences Applied to Health Products
https://orcid.org/0000-0002-8561-5586 • fernandesbaline@gmail.com
Contribution: Data curation, Formal Analysis, Investigation, Writing – original draft, and review & editing.

2 – Alliny das Graças Amaral

PhD in Animal Science
https://orcid.org/0000-0002-1418-9698 • alliny.amaral@ueg.br
Contribution: Data curation, Formal Analysis, Investigation, Methodology, Software, Supervision, Validation, Writing – original draft, and review & editing.

3 – Lílian Carla Carneiro

PhD in Cellular and Molecular Biology
https://orcid.org/0000-0003-4067-1506 • liliancarla@ufg.br
Contribution: Investigation, Writing – review & editing

4 - Plínio Lázaro Faleiro Naves
PhD in Microbiology and Parasitology
https://orcid.org/0000-0003-1936-1837 • plinionaves@ueg.br
Contribution: Conceptualization, Data curation, Formal Analysis, Funding acquisition, Investigation, Methodology, Project administration, Resources, Supervision, Validation, Writing – original draft, and review & editing.

5 - Luciana Rebelo Guilherme

PhD in Inoganic Chemistry.
https://orcid.org/0000-0002-0433-5751 • luciana.guilherme@ueg.br
Contribution: Conceptualization, Data curation, Formal Analysis, Funding acquisition, Investigation, Methodology, Project administration, Resources, Supervision, Validation, Writing – original draft, and review & editing.

How to quote this article

Barcelos, A. F., Amaral, A. das G., Carneiro, L. C., Naves, P. L. F., & Guilherme, L. R. (2025). Synthesis and antimicrobial activity of iron oxide/silver nanocomposites against *Pseudomonas aeruginosa biofilms*. *Ciencia e Natura*, 47, e84264. DOI: https://doi.org/10.5902/2179460X84264. Available in: https://doi.org/10.5902/2179460X84264